


LETTER

Open Access



Co-seismic offsets due to two earthquakes (M_w 6.1) along the Sumatran fault system derived from GNSS measurements

Takeo Ito^{1*} , Endra Gunawan², Fumiaki Kimata³, Takao Tabei⁴, Irwan Meilano², Agustan⁵, Yusaku Ohta⁶, Nazli Ismail⁷, Irwandi Nurdin⁷ and Didik Sugiyanto⁷

Abstract

Since the 2004 Sumatra–Andaman earthquake (M_w 9.2), the northwestern part of the Sumatran island has been a high seismicity region. To evaluate the seismic hazard along the Great Sumatran fault (GSF), we installed the Aceh GNSS network for the Sumatran fault system (AGNeSS) in March 2005. The AGNeSS observed co-seismic offsets due to the April 11, 2012 Indian Ocean earthquake (M_w 8.6), which is the largest intraplate earthquake recorded in history. The largest offset at the AGNeSS site was approximately 14.9 cm. Two M_w 6.1 earthquakes occurred within AGNeSS in 2013, one on January 21 and the other on July 2. We estimated the fault parameters of the two events using a Markov chain Monte Carlo method. The estimated fault parameter of the first event was a right-lateral strike-slip where the strike was oriented in approximately the same direction as the surface trace of the GSF. The estimated peak value of the probability density function for the static stress drop was approximately 0.7 MPa. On the other hand, the co-seismic displacement fields of the second event from nearby GNSS sites clearly showed a left-lateral motion on a north-east–southwest trending fault plane and supported the contention that the July 2 event broke at the conjugate fault of the GSF. We also calculated the Coulomb failure function ΔCFF caused by the first event to evaluate its effect on the second event. The results showed that the July 2 event was likely brought 0.1 MPa closer to failure by the January 21 event.

Keywords: Conjugate fault, MCMC method, Sumatran fault

Background

Since the December 26, 2004 Sumatra–Andaman earthquake (M_w 9.2), the northwestern part of the Sumatran island has been an area of high seismicity (Nalbant et al. 2005) because there have been nine earthquakes of $M_w \geq 7.5$ in the region, with four of them being responsible for triggering damaging tsunamis. The 2004 Sumatra–Andaman earthquake may have triggered the March 28, 2005 Nias–Simeulue earthquake (M_w 8.6) at the southern edge of the 2004 Sumatra–Andaman earthquake rupture area (Franke et al. 2008; Hsu et al. 2006). The September 12, 2007 Bengkulu earthquake (M_w 8.4)

and the October 25, 2010 Mentawai earthquake (M_w 7.8) occurred in the deeper (10–30 km) and shallower (<6 km) sections of the Sunda subduction zone, respectively (Gusman et al. 2010; Hill 2012). On April 11, 2012, an M_w 8.6 earthquake struck off the west coast of northern Sumatra approximately 100 km west of the Sunda trench, which is in a diffuse deformation zone where the Australian–Indian oceanic plate is cleaving in two. This event in the Indian Ocean was followed by a second earthquake (M_w 8.2) 2 h later. The two earthquakes on April 11, 2012, could have occurred as the result of a left-lateral slip on a north–northeast striking fault or a right-lateral dip on a west–northwest striking fault. The two different strike-slip faulting orientations are possible under the same tectonic stress field. Perpendicular strike-dip faults that are both compatible with the same stress field are called “conjugate faults.” The 2012 Indian Ocean

*Correspondence: takeo_ito@nagoya-u.jp

¹ Graduate School of Environmental Studies, Nagoya University, Furo-cho, Chikusa-ku, Nagoya 464-8602, Japan

Full list of author information is available at the end of the article

earthquake is the largest intraplate earthquake recorded in history (Delescluse et al. 2012). This event may provide information concerning the rheology of the oceanic asthenosphere.

Among the outstanding features of the Sunda trench system is the 1900-km-long Sumatran fault (Sieh and Natawidjaja 2000). The Great Sumatran fault (GSF) system is a major 1900-km trench-parallel strike-slip fault system with several segments. It extends the entire length of the Sumatran island and coincides geographically with the volcanic arc through most of its length. The GSF system has a right-lateral component that accommodates a significant amount of the strike-slip component of the oblique convergence between the Australian/Indian and Sunda plates (Fitch 1972; Sieh and Natawidjaja 2000; Genrich et al. 2000). Following the 2004 Sumatra–Andaman earthquake, previous studies had expected earthquakes to be triggered on the GSF (Nalbant et al. 2005; McCloskey et al. 2005; Cattin et al. 2009). The reasoning is based on the Coulomb failure function ΔCFF in the northern part of the GSF system due to the 2004 Sumatra–Andaman and 2005 Nias earthquakes (McCloskey et al. 2005; Cattin et al. 2009). Cattin et al. (2009) suggested that ΔCFF increases by approximately 2 MPa on the northwestern part of the Sumatran fault, resulting in a greater seismic hazard potential for this region that may trigger a fault slip in the northwestern part on the Sumatran fault in the near future. Such earthquakes have yet to occur, and seismic activity along the GSF has not changed greatly. McCaffrey (2009) suggested that it takes a long time for the stress changes to act in the Earth due to fluids that modify the stress field (poroelastic effects). However, the question is still under debate.

In this paper, we present the GNSS measurements of co-seismic offsets resulting from the 2012 Indian Ocean earthquake and two subsequent M_w 6.1 earthquakes that occurred in the northwestern part of the Sumatran islands. The observed co-seismic offsets due to the 2012 Indian Ocean earthquake were consistent with the rupture models derived from seismological methods. The estimated focal mechanisms for the two M_w 6.1 events from co-seismic offsets were consistent with centroid moment tensor (CMT) solutions. However, the observed co-seismic displacement close to the source region suggested the presence of conjugated fault ruptures, which were not parallel to the GSF.

GNSS observations

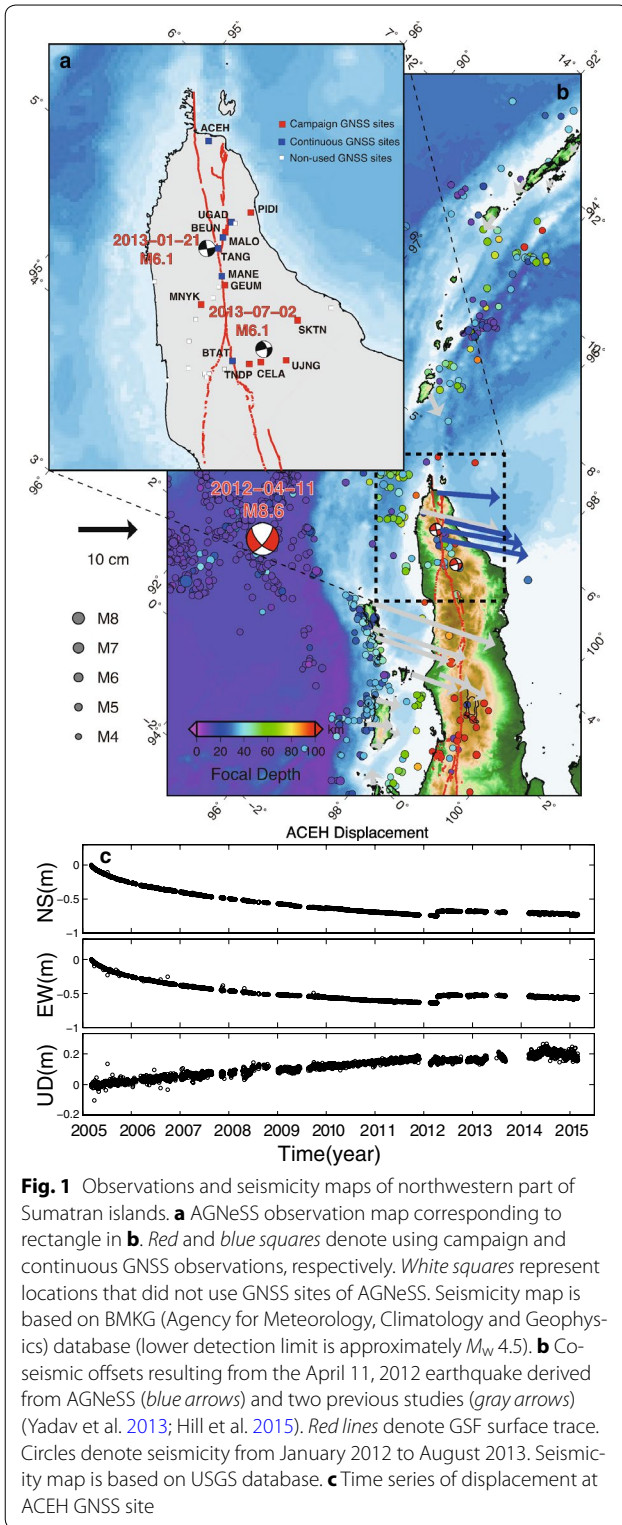
In March 2005, we established the Aceh GNSS Network for the Sumatran Fault System (AGNeSS) in the northwestern part of the Sumatran island (Ito et al. 2012; Gunawan et al. 2014). The AGNeSS consisted of seven continuous and 17 campaign GNSS sites spanning the

northwestern segment of the GSF system. In this study, we used only 14 GNSS sites, which consisted of six continuous and eight campaign GNSS sites, to observe the events (Fig. 1a). The complete observation map of the AGNeSS is shown in Fig. 1b. For continuous GNSS measurements, we used Trimble 4000SSI receivers set to sample every second. For all the campaign GNSS measurements, we used Trimble 5700 receivers and occupied each site between 24 and 48 h. We used the Bernese 5.0 software to estimate the daily positions. We included the permanent International GNSS Service (IGS) sites (KUNM, PIMO, HYDE, and COCO), the IGS final ephemeris, earth rotation parameters, ionosphere model parameters, and differential code biases for satellites and receivers. The AGNeSS observed the post-seismic deformation exceeding 90 cm for 9 years following the 2004 Sumatra–Andaman earthquake (Ito et al. 2012). Figure 1c shows the time series of displacement at the Aceh GNSS site. The horizontal offset of the 2012 Indian Ocean earthquake was over 10 cm.

Fault parameter estimation

The fault parameters (locations, strike, dip, length, width, and slip amount) are highly correlated nonlinear parameters. To estimate these fault parameters, we employed a Markov chain Monte Carlo (MCMC) method, which is a powerful method for estimating the probability density functions (PDFs) of such parameters. In this study, we used the observed co-seismic offset, focal mechanism, and magnitude from seismic waveform analyses, which provided independent information related to crustal deformation. The event focal mechanism was introduced by a priori information, which was controlled by a hyper-parameter α . The slip amount was highly correlated with the magnitude, length, and width of the fault plane. To stabilize the solution, we fixed the magnitude, which was controlled by the MCMC sample. Hence, we could control the slip amount by adjusting the magnitude, rigidity, length, and width of the fault (Hanks and Kanamori 1979). We selected the length and width of the fault using the MCMC sample, and the slip amount was automatically selected. Our objective was to find the fault parameters as PDFs. For simplicity, we assumed that the observed data were mutually independent and had errors that obeyed $N(0, E)$ and that the material was a homogeneous, elastic, and isotropic half-space in the analysis (Okada 1992). Then, we could determine the PDFs of the data as follows:

$$p(\mathbf{d}|\boldsymbol{\theta}) = (2\pi)^{-\frac{N}{2}} |\mathbf{E}|^{-\frac{1}{2}} \exp \left(-\frac{1}{2} \times (\mathbf{d} - \mathbf{G}(\boldsymbol{\theta}))^T \mathbf{E}^{-1} (\mathbf{d} - \mathbf{G}(\boldsymbol{\theta})) \right) \quad (1)$$



where N and E denote the number of observed data d and the covariance matrix, respectively (Fisher 1922). The estimated data vector $G(\theta)$ was calculated by a forward

model with fault parameter θ under an elastic half-space medium. Here we assumed that the fault parameters of an event were consistent with CMT solutions, and we incorporated this assumption into our MCMC scheme as a priori information. The CMT solutions were obtained from the US Geological Survey, National Earthquake Information Center. Specifically, we added a constraint that the slip vector from the CMT solution must follow the fault parameters:

$$0 = S(\theta) - S(\theta_{\text{CMT}}) \quad (2)$$

where $S(\theta)$ is the slip vector, which is defined by the rake, strike, and dip of the fault parameter θ . We may represent the constraint in the form of the PDF of the fault parameters θ with a hyper-parameter α . The prior PDF of the constraint Eq. (2) can be written as follows:

$$p(\theta; \alpha^2) = \frac{1}{\sqrt{2\pi\alpha^2}} \exp\left(-\frac{1}{2\alpha^2}(S(\theta) - S(\theta_{\text{CMT}}))^T(S(\theta) - S(\theta_{\text{CMT}}))\right) \quad (3)$$

Here, we incorporated a priori distribution $p(\theta; \alpha^2)$ in Eq. (3) with the data distribution $p(d|\theta)$ in Eq. (1) and obtained the posterior PDF through Bayes' theorem as follows:

$$p(\theta; \alpha^2|d) \propto p(d|\theta) \times p(\theta; \alpha^2) = \frac{1}{(\sqrt{2\pi})^{N+1} \times \sqrt{\alpha^2|E|}} \exp\left(-\frac{1}{2}\left(R(d, \theta) + \frac{1}{\alpha^2}C(\theta)\right)\right) \quad (4)$$

where

$$R(d, \theta) = (d - G(\theta))^T E^{-1} (d - G(\theta))$$

$$C(\theta) = (S(\theta) - S(\theta_{\text{CMT}}))^T (S(\theta) - S(\theta_{\text{CMT}}))$$

The posterior PDF, $p(\theta; \alpha^2|d)$, is a non-Gaussian distribution. Because a closed-form analytical expression was unavailable, we constructed a discrete representation of the posterior PDF by sampling with a MCMC method using the Metropolis–Hastings (M–H) algorithm (Metropolis et al. 1953; Hastings 1970). In the M–H algorithm, we discarded the 3.0×10^6 samples as having memory of the initial parameters and considered the subsequent 3.0×10^7 samples drawn from the posterior PDF.

Results

The AGNeSS observed the co-seismic offset due to three events, i.e., the April 11, 2012 earthquake (M_w 8.6) and the January 22 and July 2, 2013 earthquakes (M_w 6.1). In particular, the two M6-class earthquakes were the

first to occur within the AGNeSS after the AGNeSS was established.

April 11, 2012 earthquake

The April 11, 2012 Indian Ocean earthquake (M_w 8.6), the largest strike-slip earthquake ever recorded, occurred approximately 610 km southwest of Banda Aceh. Two hours later, another earthquake (M_w 8.2) occurred approximately 180 km southwest of the first (McGuire and Beroza 2012; Ishii et al. 2013). Previous studies (Yadav et al. 2013; Hill et al. 2015) reported co-seismic offsets around the Andaman–Nicobar GNSS network, which includes the Sumatran GNSS Array (SuGAR) and IGS sites. The AGNeSS also observed horizontal co-seismic offsets (Table 1). The largest horizontal offset observed by the AGNeSS was approximately 14.9 cm at the MANE site, which is located approximately 440 km from the epicenters of the 2012 Indian Ocean earthquakes. However, the vertical offsets were very small (~ 1 cm); thus, we reported only the horizontal offsets at the AGNeSS site. Figure 1b shows the horizontal displacements from the GNSS sites, which consisted of AGNeSS (blue arrows), SuGAR, and IGS sites (gray arrows) (Yadav et al. 2013; Hill et al. 2015). These offsets contained the effects of both the M_w 8.6 sequence and the M_w 8.2 aftershock. Hill et al. (2015) constructed a fine co-seismic model from high-rate GNSS time series, static GNSS displacements, and broadband teleseismic data. The co-seismic offsets at the AGNeSS sites were also consistent with the predicted offsets (Hill et al. 2015). The post-seismic deformation at ACEH 3 years after the 2012 Indian Ocean earthquake

was up to 10 cm (Fig. 1c). This post-seismic deformation may include useful information for understanding the oceanic asthenosphere, such as viscosity.

January 21, 2013 earthquake

On January 21, 2013, an M_w 6.1 earthquake occurred within the AGNeSS. The focal mechanism and location of the first event strongly suggested the occurrence of a right-lateral strike-slip on the northwest–southeast trending GSF. The event occurred close to the GSF, and the GNSS site closest to this event was <10 km away. We estimated the co-seismic offset at the AGNeSS site using a correction for post-seismic deformation due to the 2004 earthquake. In order to remove the deformation at the campaign GNSS site, we applied post-seismic deformation modeling based on Ito et al. (2012). After correction, we estimated the co-seismic offset due to the event. The vertical errors at the campaign GNSS site that were attributed to the resetting of the tripod and the daily positions were estimated to be several centimeters and 0.8 cm, respectively. The predicted co-seismic displacement for the vertical component was approximately 3.5 cm of subsidence at the GEUM site (Fig. 4a). However, the typical error of the vertical component was larger than the predicted co-seismic offset. In this study, we did not use the vertical component of the GNSS observations for the data analysis. The maximum co-seismic offset in the horizontal component was 7.4 cm at the GEUM site (Table 1). This co-seismic offset was oriented in a south-east direction, which was consistent with the right-lateral strike-slip on the GSF.

Table 1 Observed co-seismic offsets determined by AGNeSS

GNSS site	Latitude	Longitude	North (cm)	East (cm)	Event
ACEH	5.57°N	95.37°E	6.21 ± 0.82	8.72 ± 0.82	April 2012
UGAD	5.22°N	95.87°E	5.32 ± 0.91	10.51 ± 0.81	April 2012
TANG	5.02°N	95.92°E	7.01 ± 0.93	12.31 ± 0.92	April 2012
MANE	4.88°N	96.07°E	7.26 ± 0.94	13.12 ± 0.90	April 2012
GEUM	4.84°N	96.13°E	−4.14 ± 1.04	6.14 ± 1.21	January 2013
MANE	4.88°N	96.07°E	−5.15 ± 1.02	4.97 ± 1.03	January 2013
TANG	5.02°N	95.92°E	0.13 ± 0.97	−0.65 ± 0.91	January 2013
MALO	5.10°N	95.89°E	−0.32 ± 0.99	−0.38 ± 0.98	January 2013
BEUN	5.14°N	95.88°E	0.54 ± 1.14	1.09 ± 1.43	January 2013
UGAD	5.22°N	95.87°E	−1.31 ± 0.89	0.19 ± 0.98	January 2013
PIDI	5.37°N	95.93°E	0.64 ± 1.14	−0.50 ± 1.27	January 2013
MNYK	4.63°N	96.08°E	2.42 ± 1.42	−1.82 ± 1.24	January 2013
SKTN	4.99°N	96.69°E	0.80 ± 1.04	0.40 ± 1.21	July 2013
UJNG	4.71°N	96.82°E	0.64 ± 1.23	1.42 ± 1.34	July 2013
CELA	4.58°N	96.68°E	1.35 ± 1.43	4.31 ± 1.32	July 2013
TNDP	4.52°N	96.63°E	1.43 ± 1.25	2.20 ± 1.40	July 2013
BTAT	4.46°N	96.52°E	1.44 ± 0.99	0.18 ± 0.98	July 2013

July 2, 2013 earthquake

The epicenter of the July 2 event was approximately 25 km east of the GSF, and the USGS focal mechanism was very similar to that of the January 21 event (Fig. 2). We estimated the stress drop due to the July 2 event; however, the stress drop is strongly dependent on the fault size, and the fault length and width were difficult to determine because the current AGNeSS site distribution around the epicenter of the July 2 event only covered one side. Consequently, the fault length could not be determined (Fig. 3). Given the limitation of the AGNeSS site distribution, there were two possible approximations for the rake and strike of the July 2 event from the MCMC estimation. The rake and strike correlated with the source location, which was either on the northwest or on the southeast side of the aligned GNSS site around the July 2 event. As a result, we could not determine which set of the two possible fault parameters better fit the co-seismic offsets. However, the observation of landslides and

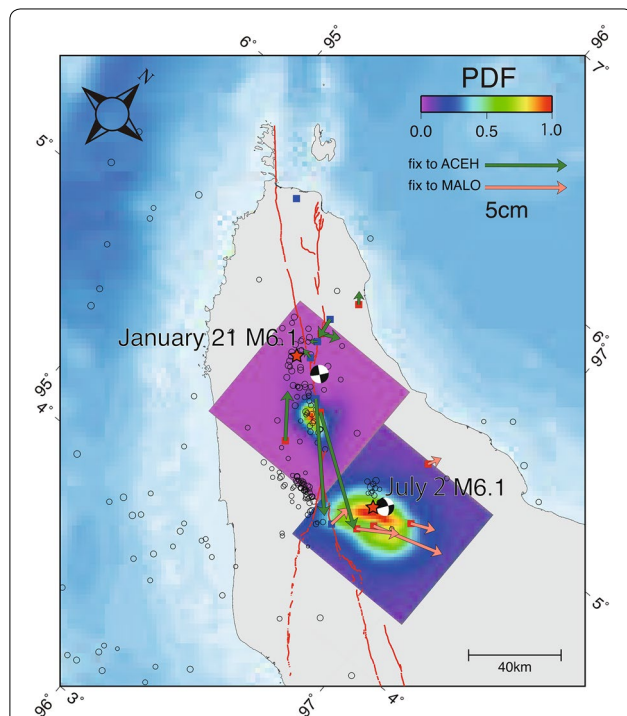


Fig. 2 Marginal posterior PDFs of source locations due to two events. PDFs were normalized by each peak value. The observed co-seismic offsets were derived from AGNeSS around northwestern part of Sumatran islands. Green and orange arrows denote the observed co-seismic offsets resulting from January 21 and July 2, 2013 earthquakes, respectively. The observed co-seismic offsets of January 21 and July 2 events were relative movements to permanent ACEH and MALO GNSS sites, respectively. Seismicity was based on BMKG database. Focal mechanisms of two events referenced USGS data. Red stars refer to epicenters of two events

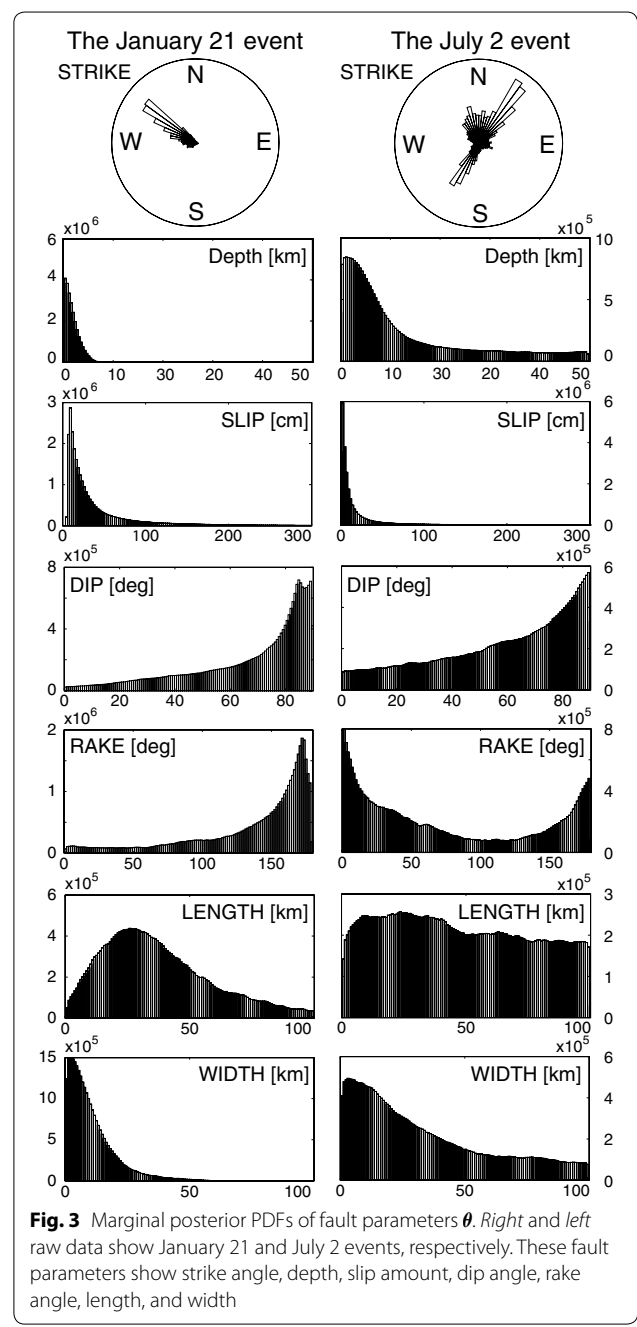


Fig. 3 Marginal posterior PDFs of fault parameters θ . Right and left raw data show January 21 and July 2 events, respectively. These fault parameters show strike angle, depth, slip amount, dip angle, rake angle, length, and width

damaged buildings resulting from this event suggested that the source was located on the northwest side of the aligned GNSS site. Thus, the strike of the July 2 event was assumed to be oriented in an east–west direction, which was inconsistent with the strike direction of the GSF. The strike of the July 2 event may correspond to a conjugate fault, though there is no evidence at the ground surface for the existence of a conjugate fault system associated with the GSF.

Fig. 4 **a** Estimated co-seismic offsets due to January 21 event. *Map colors indicate vertical displacement.* **b** Marginal posterior PDF of stress drop due to January 21 event. **c** Static Coulomb stress change (effective friction 0.4) of July 2 event resulting from January 21 event

Discussion

Estimated fault parameters

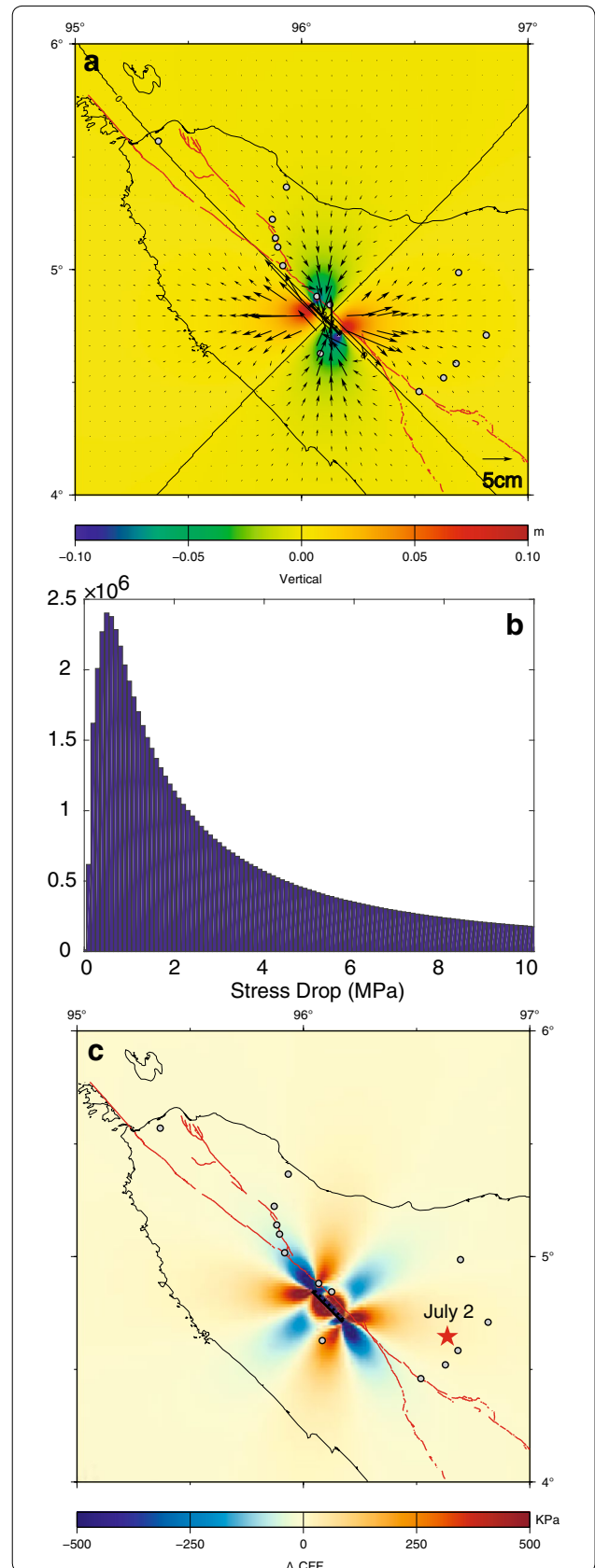
We estimated the focal mechanisms for two events from the observed co-seismic offsets derived from the GNSS measurements. Figure 2 shows the PDF of the source locations for the two events that occurred in 2013. Fortunately, the source region of the January 21 event was covered by the GNSS site. Therefore, the estimated source locations of the January 21 event were more accurate than those of the July 2 event. The PDF distribution of the source location for the January 21 event slightly extended in the northwest–southeast direction and depended on the distribution of the GNSS site. The estimated location of the January 21 event derived from the co-seismic offsets was approximately 25 km southeast of the epicenter determined by the USGS, which was close to the GSF. The centroid of the focal mechanism was located approximately 10 km east of the epicenter. These results indicated that the main slip was southeast of the epicenter. Our result was a reasonable estimate of the damaged area and aftershock region. The focal mechanism of the January 21 event was consistent with a right-lateral fault, where the strike was oriented in approximately the same direction as the surface trace of the GSF (Fig. 3). Figure 4a shows the co-seismic displacement due to the January 21 event. The co-seismic offsets at the northwest part of the AGNeSS were <2 cm (Fig. 2) because these GNSS sites were located along the extended nodal fault plane, where the direction and amplitude of the co-seismic offsets changed quite rapidly. This indicated that the estimated strike direction was nearly unique (Fig. 3). The January 21 event broke a small segment along the GSF.

Static stress drop

The stress drop is a fundamental parameter of earthquake dynamics. If we assume that the January 21 event was due to a strike-slip, then the static stress drop $\Delta\sigma$ can be expressed as follows:

$$\Delta\sigma = \frac{2}{\pi} \mu \left(\frac{\bar{D}}{w} \right) \tag{5}$$

where μ , \bar{D} and w represent the rigidity, the average displacement and width of the fault, respectively (Parsons et al. 1988). We employed the value of rigidity as 30 GPa. Figure 4b shows the PDF of the static stress drop. The peak and mean values of the PDF for the static stress



drop were approximately 0.7 and 2.0 MPa, respectively. These values were approximately equal to one or one-third of ΔCFF due to a series of Sunda trench events (Cattin et al. 2009). Typically, the static stress drop of inland earthquakes ranges from 1 to 10 MPa, and there is no dependence of the stress drop on the seismic moment (e.g., Baltay et al. 2011). The estimated stress drop in the current work was relatively small compared to those found in other studies (e.g., Allmann and Shearer 2009). In this region, Ito et al. (2012) observed that the creep region, which is close to the broken segment, may be relatively weaker than other regions. Our estimated low stress drop may thus be consistent with that reported by Ito et al. (2012).

ΔCFF

We sought to understand the source and consequences of the remarkable increase in seismicity along the GSF. We attempted to explain the observations by static stress transfer and to explain that the July 2 event was an effect of the January 21 event. The static Coulomb failure function (or stress change) caused by the fault slip may be calculated through the following equation: $\Delta\text{CFF} = \Delta\tau + \mu\Delta\sigma_n$, where $\Delta\tau$ is the shear stress change caused by the January 21 event, $\Delta\sigma_n$ is the fault-normal stress change (positive when unclamped), and μ is the effective coefficient of friction (King et al. 1994; Harris 1998). The static stress change produced by the January 21 event was estimated based on an equation proposed by Okada (1992), assuming an elastic dislocation in a half-space with a rigidity of 30 GPa and a Poisson's ratio of 0.25. To evaluate the effect on the subsequent July 2 event, the regional stress change caused by the January 21 event was calculated using the fault parameters estimated by the MCMC method. The strike of the July 2 event was oriented in a north-east–southwest direction, which was inconsistent with the direction of the GSF. Figure 4c shows the Coulomb stress change of the July 2 event resulting from the January 21 event. The static Coulomb stress change at the epicenter of the July 2 event increased by approximately 0.1 MPa. This value was smaller than ΔCFF due to a series of Sunda trench events, which produced a stress change of approximately 1.6 MPa. Although ΔCFF due to the January event was very small (approximately 0.1 MPa) and corresponded to a small percentage of the typical stress drop of inland earthquakes (1–10 MPa), the January 21 event contributed to increasing the risk of the July 2 event. However, we could not find other evidence of a clear relationship between the two events. As a result, we could only suggest that the July 2 event was brought 0.1 MPa closer to failure by the January 21 event.

Conclusions

We detected co-seismic offsets resulting from three events, i.e., the April 11, 2012 Indian Ocean earthquake and the January 21 and July 2, 2013, events detected by the AGNeSS in the northwestern part of the Sumatran islands. The observed co-seismic offsets due to the 2012 Indian Ocean earthquake, among which the largest offset at the AGNeSS was 14.9 cm in a north-northeast direction, were consistent with otherwise estimated co-seismic models (Hill et al. 2015). The largest observed co-seismic offset resulting from the 2012 Indian Ocean earthquake at the AGNeSS was 14.9 cm in a north-northeast direction. The AGNeSS also observed co-seismic offsets due to two M_w 6.1 events around the GSF. We investigated the focal mechanisms and static stress drop using the MCMC method and the static stress change resulting from the January 21 event. We identified that the January 21, 2013, event broke along the GSF segments and that the July 2 event did not break along the GSF segments. The observed displacement supported the contention that the July 2 event broke at the GSF conjugate fault. The July 2 event was brought 0.1 MPa closer to failure by the January 21 event.

Authors' contributions

TI provided the MCMC and GNSS analysis. EG analyzed GNSS data. FK, TT, IM, AA, YO, NI, IN and DS made the GNSS observations. All authors read and approved the final manuscript.

Author details

¹ Graduate School of Environmental Studies, Nagoya University, Furo-cho, Chikusa-ku, Nagoya 464-8602, Japan. ² Geodesy Research Division, Bandung Institute of Technology, Jl. Ganesha, Bandung, Indonesia. ³ Tono Research Institute of Earthquake Science, Akiyo-cho, Mizunami, Japan. ⁴ Department of Applied Science, Kochi University, Akebono-cho, Kochi, Japan. ⁵ Center of Technology for Natural Resources Inventory, BPPT, Thamrin, Jakarta, Indonesia. ⁶ Graduate School of Science, Tohoku University, Aramaki, Aoba-ku, Sendai, Japan. ⁷ Faculty of Mathematics and Natural Sciences, Syiah Kuala University, Jl. Syech Abdurrauf, Darussalam, Banda Aceh, Indonesia.

Acknowledgements

We thank two anonymous referees for their careful reading of our manuscript and their numerous constructive suggestions that helped to improve this paper. This work was supported by Grants-in-Aid for Scientific Research from the Ministry of Education, Culture, Sports, Science and Technology, Japan (Nos. 24403005, 23740337). Some figures were prepared using the generic mapping tools (GMT) package (Wessel and Smith 1998).

Competing interests

The authors declare that they have no competing interests.

Received: 15 October 2015 Accepted: 17 March 2016

Published online: 12 April 2016

References

- Allmann BP, Shearer PM (2009) Global variations of stress drop for moderate to large earthquakes. *J Geophys Res Solid Earth*. doi:10.1029/2008JB005821
- Baltay A, Ide S, Prieto G, Beroza G (2011) Variability in earthquake stress drop and apparent stress. *Geophys Res Lett* 38:06303. doi:10.1029/2011GL046698

- Cattin R, Chamot-Rooke N, Pubellier M, Rabaute A, Delescluse M, Vigny C, Fleitout L, Dubernet P (2009) Stress change and effective friction coefficient along the Sumatra–Andaman–Sagaing fault system after the 26 December 2004 ($M_w = 9.2$) and the 28 March 2005 ($M_w = 8.7$) earthquakes. *Geochem Geophys Geosyst*. doi:10.1029/2008gc002167
- Delescluse M, Chamot-Rooke N, Cattin R, Fleitout L, Trubienko O, Vigny C (2012) April 2012 intra-oceanic seismicity off Sumatra boosted by the Banda-Aceh megathrust. *Nature* 490(7419):240–244. doi:10.1038/Nature11520
- Fisher RA (1922) On the mathematical formulations of theoretical statics. *Philos Trans R Soc Lond* 222:309–368
- Fitch TJ (1972) Plate convergence, transcurrent faults, and internal deformation adjacent to southeast Asia and western Pacific. *J Geophys Res* 77(23):4432–4460. doi:10.1029/Jb077i023p04432
- Franke D, Schnabel M, Ladage S, Tappin DR, Neben S, Djajadihardja YS, Müller C, Kopp H, Gaedicke C (2008) The great Sumatra–Andaman earthquakes—imaging the boundary between the ruptures of the great 2004 and 2005 earthquakes. *Earth Planet Sci Lett* 269:118–130
- Genrich JF, Bock Y, McCaffrey R, Prawirodirdjo L, Stevens CW, Puntodewo SSO, Subarya C, Wdowinski S (2000) Distribution of slip at the northern Sumatran fault system. *J Geophys Res* 105(B12):28327–28341
- Gunawan E, Sagiya T, Ito T, Kimata F, Tabei T, Ohta Y, Meilano I, Abidin HZ, Agustan Nurdin I, Sugiyanto D (2014) A comprehensive model of postseismic deformation of the 2004 Sumatra–Andaman earthquake deduced from GPS observations in northern Sumatra. *J Asian Earth Sci* 88:218–2013229. doi:10.1016/j.jseaes.2014.03.016
- Gusman AR, Tanioka Y, Kobayashi T, Latief H, Pandoe W (2010) Slip distribution of the 2007 Bengkulu earthquake inferred from tsunami waveforms and InSAR data. *J Geophys Res*. doi:10.1029/2010JB007565
- Hanks TC, Kanamori H (1979) Moment magnitude scale. *J Geophys Res* 84(Nb5):2348–2350
- Harris RA (1998) Introduction to special section: stress triggers, stress shadows, and implications for seismic hazard. *J Geophys Res* 103(B10):24347–24358. doi:10.1029/98jb01576
- Hastings WK (1970) Monte-Carlo sampling methods using Markov chains and their applications. *Biometrika* 57(1):97–109
- Hill E (2012) The 2010 M_w 7.8 Mentawai earthquake: very shallow source of a rare tsunami earthquake determined from tsunami field survey and near-field GPS data. *J Geophys Res* 117(06402):2012J. doi:10.1029/B009159
- Hill EM, Yue H, Barbot S, Lay T, Tapponnier P, Hermawan I, Hubbard J, Banerjee P, Feng L, Natawidjaja D, Sieh K (2015) The 2012 M_w 8.6 Wharton Basin sequence: a cascade of great earthquakes generated by near-orthogonal, young, oceanic mantle faults. *J Geophys Res Solid Earth* 120(B12316):3723–3747. doi:10.1002/2014JB011703
- Hsu YJ, Simons M, Avouac JP, Galetzka J, Sieh K, Chlieh M, Natawidjaja D, Prawirodirdjo L, Bock Y (2006) Frictional afterslip following the 2005 Nias–Simeulue earthquake, Sumatra. *Science* 312(5782):1921–1926
- Ishii M, Kiser E, Geist EL (2013) M_w 8.6 Sumatran earthquake of 11 April 2012 rare seaward expression of oblique subduction. *Geology* 41(3):319–322. doi:10.1130/G33783.1
- Ito T, Gunawan E, Kimata F, Tabei T, Simons M, Meilano I, Agustan Ohta Y, Nurdin I, Sugiyanto D (2012) Isolating along-strike variations in the depth extent of shallow creep and fault locking on the northern Great Sumatran Fault. *J Geophys Res*. doi:10.1029/2011jb008940
- King GCP, Stein RS, Lin J (1994) Static stress changes and the triggering of earthquakes. *Bull Seismol Soc Am* 84(3):935–953
- McCaffrey R (2009) The tectonic framework of the Sumatran subduction zone. *Annu Rev Earth Planet Sci* 37:345–366. doi:10.1146/annurev.earth.031208.100212
- McCloskey J, Nalbant SS, Steacy S (2005) Indonesian earthquake: earthquake risk from co-seismic stress. *Nature* 434(7031):291–291
- McGuire JJ, Beroza GC (2012) A rogue earthquake off Sumatra. *Science* 336(6085):1118–1119. doi:10.1126/Science.1223983
- Metropolis N, Rosenbluth AW, Rosenbluth MN, Teller AH, Teller E (1953) Equation of state calculations by fast computing machines. *J Chem Phys* 21(6):1087–1092
- Nalbant SS, Steacy S, Sieh K, Natawidjaja D, McCloskey J (2005) Earthquake risk on the Sunda trench. *Nature* 435(7043):756–757
- Okada Y (1992) Internal deformation due to shear and tensile faults in a half-space. *Bull Seismol Soc Am* 82(2):1018–1040
- Parsons ID, Hall JF, Lyzenga GA (1988) Relationships between the average offset and the stress drop for two-dimensional and 3-dimensional faults. *Bull Seismol Soc Am* 78(2):931–945
- Sieh K, Natawidjaja D (2000) Neotectonics of the Sumatran fault, Indonesia. *J Geophys Res* 105(B12):28295–28326
- Wessel P, Smith WHF (1998) New, improved version of generic mapping tools released. *Eos Trans Am Geophys Union* 79(47):579–579. doi:10.1029/98EO00426
- Yadav RK, Kundu B, Gahalaut K, Catherine J, Gahalaut VK, Ambikapathy A, Naidu MS (2013) Coseismic offsets due to the 11 April 2012 Indian Ocean earthquakes (M_w 8.6 and 8.2) derived from GPS measurements. *Geophys Res Lett* 40:3389–3393

Submit your manuscript to a SpringerOpen® journal and benefit from:

- Convenient online submission
- Rigorous peer review
- Immediate publication on acceptance
- Open access: articles freely available online
- High visibility within the field
- Retaining the copyright to your article

Submit your next manuscript at ► springeropen.com